

# Evolution of the average steepening factor for nonlinearly propagating waves

Michael B. Muhlestein,<sup>a)</sup> Kent L. Gee, Tracianne B. Neilsen, and Derek C. Thomas  
*Department of Physics and Astronomy, Brigham Young University, Provo, Utah 84602*

(Received 7 July 2014; revised 11 December 2014; accepted 13 January 2015)

Difficulties arise in attempting to discern the effects of nonlinearity in near-field jet-noise measurements due to the complicated source structure of high-velocity jets. This article describes a measure that may be used to help quantify the effects of nonlinearity on waveform propagation. This measure, called the average steepening factor (ASF), is the ratio of the average positive slope in a time waveform to the average negative slope. The ASF is the inverse of the wave steepening factor defined originally by Gallagher [AIAA Paper No. 82-0416 (1982)]. An analytical description of the ASF evolution is given for benchmark cases—initially sinusoidal plane waves propagating through lossless and thermoviscous media. The effects of finite sampling rates and measurement noise on ASF estimation from measured waveforms are discussed. The evolution of initially broadband Gaussian noise and signals propagating in media with realistic absorption are described using numerical and experimental methods. The ASF is found to be relatively sensitive to measurement noise but is a relatively robust measure for limited sampling rates. The ASF is found to increase more slowly for initially Gaussian noise signals than for initially sinusoidal signals of the same level, indicating the average distortion within noise waveforms occur more slowly.

© 2015 Acoustical Society of America. [<http://dx.doi.org/10.1121/1.4906584>]

[OU]

Pages: 640–650

## I. INTRODUCTION

High-velocity jets are loud, extended, directional noise sources. Far from the source region, nonlinear effects need to be accounted for to predict the levels and spectral properties of the propagated noise.<sup>1–4</sup> However, it is not clear whether nonlinear propagation effects are important close to the source, or, if not, at what distance nonlinear effects begin to be important. Several measures of the effect of nonlinearity on a waveform have been proposed and reported. For instance, analyzing spectral variations relative to an assumed linear response, such as second-harmonic growth (like Pernet and Payne<sup>5</sup> and Rudenko<sup>6</sup>), can help identify nonlinear processes. In addition, higher-order spectral techniques have been used to study nonlinear noise evolution. These consist of a pressure/squared-pressure quad spectral density<sup>1,2,7–12</sup> that is related to the parametric source generation in the Burgers equation, and bispectral analysis.<sup>3,4,13</sup> Furthermore, a great deal of literature discusses the limiting and asymptotic cases of the spectra (and associated correlation functions) of propagating noise, both narrow and broadband.<sup>6,14–16</sup> While other potentially useful measures of the importance of nonlinearity have been defined, not all of these measures have been thoroughly documented. The purpose of this paper is to document analytically, numerically, and experimentally obtained values of a statistically based metric, called the average steepening factor (ASF), for waveforms propagating with prominent nonlinear effects.

The nonlinear propagation phenomenon of waveform steepening may be characterized by both the statistical and

spectral features of the noise. Rudenko and Chirkin<sup>17</sup> and Webster and Blackstock<sup>18</sup> showed that the probability density function of the waveform remains stationary until shocks form, which suggests that useful measures might be based on the temporal rates of change of the pressure. The statistics (i.e., skewness and/or kurtosis) of the waveform time derivative have been used to characterize the nonlinearity for initial sinusoids,<sup>19</sup> noise in a plane-wave tube,<sup>20</sup> and jet<sup>10,21–26</sup> and rocket<sup>27,28</sup> noise. Baars and Tinney<sup>11</sup> have recently investigated a shock detection algorithm in the context of supersonic jet noise propagation for such metrics as number of shocks per unit time.

Another metric, which was proposed by Gallagher<sup>29</sup> in 1982 and revived by Baars and Tinney,<sup>11</sup> is the wave steepening factor (WSF), defined as the ratio of the magnitude of the mean negative slope to the mean positive slope of a waveform. In mathematical terms,

$$\text{WSF} = \frac{|E[\dot{p}^-]|}{E[\dot{p}^+]}, \quad (1)$$

where  $E[\dot{p}^-]$  is the expectation value of the negative slopes and  $E[\dot{p}^+]$  is the expectation value of the positive slopes in a waveform. Gallagher introduced the metric by noting that a pure sine wave has a WSF of one and a sawtooth wave has a WSF of zero, and then presented the WSFs of measured jet noise waveforms along with several other metrics. Gallagher compared the WSF at different measurement locations to make qualitative conclusions about the importance of nonlinearity in jet noise propagation. More recently, Baars *et al.*<sup>30,31</sup> used the WSF in addition to the skewness of the pressure time derivatives to study the importance of nonlinearity in model-scale, fully expanded, unheated Mach 3 jet

<sup>a)</sup>Author to whom correspondence should be addressed. Electronic mail: [mimuhle@gmail.com](mailto:mimuhle@gmail.com)

noise. In particular, they found that the WSF and the skewness of the pressure time derivatives both suggest that nonlinearity is not a dominant feature of near-field, model-scale jet noise propagation. These findings were largely based on a qualitative interpretation that the metrics lacked significant variation over space.

This paper introduces the average steepening factor (ASF), defined as the reciprocal of the WSF. Though potentially confusing, we have chosen to redefine this measure in a more intuitive and descriptive fashion so that it increases, rather than decreases, with increasing manifestations of nonlinear propagation. As part of our analysis, we give a more complete description of the meaning of the ASF, its behavior in limiting and realistic cases, and examine its behavior when applied to measured data.<sup>32</sup> In Sec. II the ASF is calculated analytically for two benchmark cases—propagation without linear attenuation as represented by the Earnshaw solution with weak-shock theory, and propagation with thermoviscous attenuation as represented by the Khokhlov solution.<sup>33</sup> In Sec. III we describe the effects of finite sampling rates and measurement noise on the estimation of the ASF. Finally, in Sec. IV we analyze numerical and experimental measurements of high-amplitude noise propagation in a plane wave tube-environment. From these numerical and physical experiments, we find the ASF quantifies the time-averaged effects of nonlinearity on a propagating waveform.

## II. ANALYTIC FORMS OF THE AVERAGE STEEPENING FACTOR

Analytical expressions corresponding to limiting cases of physical models often shed light on how a system will behave in more general, complicated scenarios. For this reason, we seek an analytical expression for the evolution of the average steepening factor (ASF) of a waveform as it propagates. As mentioned in Sec. I, the ASF is the inverse of the wave steepening factor, or in mathematical form,

$$\text{ASF} = \frac{1}{\text{WSF}} = \frac{E[\dot{p}^+]}{|E[\dot{p}^-]|}. \quad (2)$$

For a periodic signal the average negative slope is

$$E[\dot{p}^-] = -\frac{P}{T_{\text{neg}}} \quad (3)$$

and the average positive slope is

$$E[\dot{p}^+] = \frac{P}{T_{\text{pos}}}, \quad (4)$$

where  $P$  is the pressure difference between the maxima and minima within a period,  $T_{\text{neg}}$  is the duration of the negative slope during a period, and  $T_{\text{pos}}$  is the duration of the positive slope during a period. Since  $P$  cancels in the ratio of the expectation values, we find the ASF of a periodic signal depends only upon the duration of positive and negative slopes within a single period, and not the magnitude of the pressure rise or fall. This means that even with the presence

of discontinuities in a waveform, which have infinite slope, it is possible that the ASF will be finite. To aid the qualitative understanding of the ASF, one period of an initially sinusoidal plane wave of frequency  $\omega$  at several values of  $\sigma$ , the distance from the source divided by the distance at which the first shocks form, are displayed as a function of the retarded time  $\tau$  in Fig. 1. The initial waveform has an ASF value of exactly 1. By  $\sigma = 1/2$ , the ASF has nearly reached 2. At the shock formation distance, the ASF is only 4.5, despite the presence of a shock at  $\omega\tau = 0$ . Once all of the pressure rise in a period is found inside the shock, at  $\sigma = \pi/2$ , the ASF diverges.

The duration of positive and negative slopes, and therefore the ASF, may be found exactly for initially sinusoidal plane waves propagating without linear absorption at any distance from the source using the Earnshaw solution augmented with weak-shock theory.<sup>33</sup> In addition, the ASF for an initially sinusoidal plane wave propagating with thermoviscous losses may be estimated for a portion of its propagation by considering the Khokhlov solution.<sup>33</sup> These analytical forms of the ASF of an initially sinusoidal plane wave are presented below.

### A. Earnshaw solution

The Earnshaw solution is an implicit solution to the inviscid Burgers equation, which models plane wave propagation of acoustic signals prior to shock formation. The Earnshaw solution may be written as

$$p = f(\phi),$$

$$\phi = \tau + \frac{\beta}{\rho_0 c_0^3} x f(\phi), \quad (5)$$

where  $p$  is the acoustic pressure,  $f(t)$  is the pressure function at the source,  $\phi$  is the Earnshaw phase variable,  $\tau$  is the retarded time,  $x$  is the distance from the source,  $c_0$  is the small-signal sound speed,  $\beta$  is the coefficient of nonlinearity,

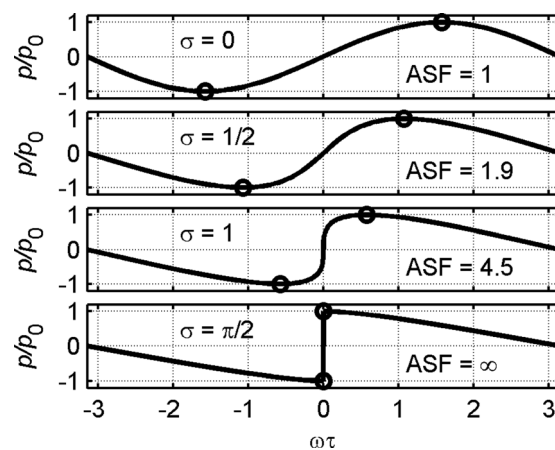


FIG. 1. A single period of an initially sinusoidal plane pressure wave at four values of the dimensionless distance  $\sigma$  (0, 1/2, 1, and  $\pi/2$ ), along with their respective values of the average steepening factor (ASF). The pressure  $p$  normalized by the initial amplitude  $p_0$  is plotted as a function of the dimensionless time  $\omega\tau$ , with  $\omega$  being the source frequency and  $\tau$  being the retarded time. The circles denote the location of the maximum and minimum amplitude in the period shown.

and  $\rho_0$  is the ambient density.<sup>33</sup> Equation (5) may be written parametrically as

$$(\tau, p) = \left( \phi - \frac{\beta}{\rho_0 c_0^3} x f(\phi), f(\phi) \right), \quad (6)$$

which should be read as (retarded time of arrival, pressure amplitude). The Earnshaw solution becomes multivalued at a distance  $x = \bar{x} \equiv \rho_0 c_0^3 / \beta f(\tau)$ , and beyond this point the Earnshaw solution ceases to give physical predictions. After  $\bar{x}$ , weak-shock theory may be used in tandem with the Earnshaw solution to describe the propagation.

To find an analytical expression for the ASF using the Earnshaw solution, we consider a periodic signal that contains only one peak and one trough per period. The arrival times of the peak and trough are denoted as  $\tau_{\max}(x)$  and  $\tau_{\min}(x)$  at a distance  $x$  from the source. Since the pressure amplitude value in Eq. (6) does not change with distance, then

$$\begin{aligned} \tau_{\max}(x) &= \tau_{\max}(0) - \frac{\beta f(\tau_{\max}(0))}{\rho_0 c_0^3} x, \\ \tau_{\min}(x) &= \tau_{\min}(0) - \frac{\beta f(\tau_{\min}(0))}{\rho_0 c_0^3} x. \end{aligned} \quad (7)$$

The duration of the positive slope within a single period is then given as

$$\tau_{\text{pos}}(x) = \tau_{\max}(x) - \tau_{\min}(x), \quad (8)$$

where, without loss of generality, we have assumed that  $\tau_{\max} > \tau_{\min}$ . If the period is  $T$ , then the duration of the negative slope within a single period is simply  $\tau_{\text{neg}}(x) = T - \tau_{\text{pos}}(x)$ .

For the initially sinusoidal case,  $f(\tau) = p_0 \sin(\omega\tau)$ ,  $\tau_{\max}(0) = \pi/2\omega$ , and  $\tau_{\min}(0) = -\pi/2\omega$  for the period  $\tau \in (-\pi/\omega, \pi/\omega]$ , which implies  $T = 2\pi/\omega$ . This means that

$$\tau_{\text{pos}}(x) = \frac{\pi}{\omega} - 2 \frac{\beta p_0}{\rho_0 c_0^3} x \quad (9)$$

and

$$\tau_{\text{neg}}(x) = \frac{2\pi}{\omega} - \left( \frac{\pi}{\omega} - 2 \frac{\beta p_0}{\rho_0 c_0^3} x \right) = \frac{\pi}{\omega} + 2 \frac{\beta p_0}{\rho_0 c_0^3} x. \quad (10)$$

Thus, the ASF is given as

$$\text{ASF} = \frac{\tau_{\text{neg}}(x)}{\tau_{\text{pos}}(x)} = \frac{\pi + 2\sigma}{\pi - 2\sigma}, \quad (11)$$

where  $\sigma = x/\bar{x}$  and  $\bar{x} = \rho_0 c_0^3 / \beta p_0 \omega$  is the shock formation distance for an initially sinusoidal signal. At  $\sigma = \pi/2$  the arrival times  $\tau_{\max}$  and  $\tau_{\min}$  are equal to each other for a given period and the pressure rise is entirely represented as a shock for the remainder of the propagation.<sup>34</sup> The evolution of the ASF according to the Earnshaw solution for all  $x \geq 0$  may be written as

$$\text{ASF} = \begin{cases} \frac{\pi + 2\sigma}{\pi - 2\sigma}, & 0 < \sigma < \frac{\pi}{2} \\ \infty, & \sigma \geq \frac{\pi}{2}, \end{cases} \quad (12)$$

which is plotted in Fig. 2 as a function of  $\sigma$ . For very small values of  $\sigma$ , the  $\text{ASF} \approx 1 + 4\sigma/\pi$ , and for  $\sigma \rightarrow \pi/2$ , the  $\text{ASF} \approx \pi/(\pi - 2\sigma)$ . There is no noticeable change in the behavior of the ASF near  $\sigma = 1$ , the shock formation distance, because the peaks and troughs are still separated by a positive time determined by the Earnshaw solution despite the presence of a shock in the waveform. At  $\sigma = \pi/2$  the Earnshaw solution predicts that the peaks and troughs arrive at the same time, causing  $E[p^+] \rightarrow \infty$  and the ASF to diverge. Similarly, for all  $\sigma > \pi/2$  the positive slopes are represented by shocks, so the ASF remains infinite.

## B. Khokhlov solution

Waves propagating through thermoviscous media cannot generate true discontinuities, and therefore never have an infinite ASF value. The evolution of arbitrary waveforms propagating with thermoviscous absorption may be found exactly using the Cole-Hopf transformation, which yields the Mendousse solution in the case of an initially sinusoidal signal.<sup>35</sup> However, because the Mendousse solution is written in the form of a ratio of infinite series it is difficult to work with analytically, so several approximations have been made to simplify it. One approximation that is particularly useful in the present study is the Khokhlov solution.<sup>33</sup> The Khokhlov solution describes the evolution of an initially sinusoidal signal propagating from the location that weak shocks form,  $\sigma = 3$ , to the distance where absorption again dominates the propagation,  $\sigma = l_\alpha$ , where  $l_\alpha$  is a characteristic absorption length.<sup>33</sup> Usually,  $l_\alpha = 1/\alpha$ , where  $\alpha$  is the absorption coefficient for the fundamental frequency.

The Khokhlov solution is given as

$$p(\tau) = \frac{p_0}{1 + \sigma} \left[ -\omega\tau + \pi \tanh \left( \frac{\pi\Gamma}{2(1 + \sigma)} \omega\tau \right) \right], \quad (13)$$

$$\Gamma > \sigma > 3,$$

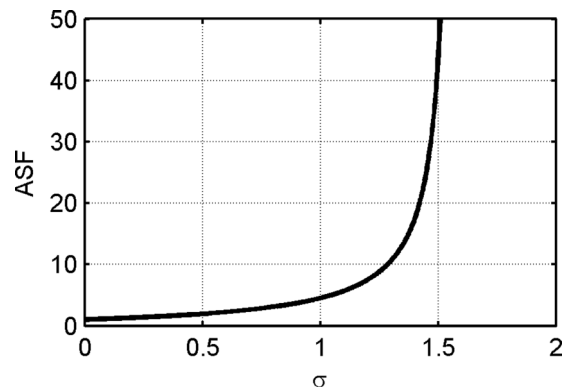


FIG. 2. Analytic expression for the average steepening factor (ASF) of an initially sinusoidal plane wave from the Earnshaw solution as a function of  $\sigma$ , the distance from the source divided by the shock formation distance.

where  $\Gamma = l_\alpha/\bar{x}$  is the Gol'dberg number. The Khokhlov solution only models the period  $-\pi < \omega\tau < \pi$ .

Blackstock<sup>36</sup> found the duration of the positive slope of the Khokhlov solution to be

$$\Delta\tau_{\text{pos}} = \frac{2\pi 2(1+\sigma)}{\omega \pi^2 \Gamma} \cosh^{-1} \sqrt{\frac{\pi^2 \Gamma}{2(1+\sigma)}}. \quad (14)$$

The corresponding duration of the negative slope is the period minus the duration of the positive slope, which is

$$\Delta\tau_{\text{neg}} = \frac{2\pi}{\omega} - \Delta\tau_{\text{pos}}. \quad (15)$$

Therefore, the analytical expression for the ASF of the Khokhlov solution is

$$\text{ASF} = \frac{\pi^2 \Gamma / 2(1+\sigma)}{\cosh^{-1} \sqrt{\pi^2 \Gamma / 2(1+\sigma)}} - 1. \quad (16)$$

(It may be useful to note that the ASF of the Khokhlov solution is approximately equal to the acoustics Reynolds number, which in this regime is the ratio of the period to the shock width.<sup>14</sup>) For large values of  $\Gamma$  and for  $\sigma$  close to 3, Eq. (16) may be approximated as

$$\text{ASF} \approx \frac{4(1+\sigma)}{\pi^2 \Gamma} \frac{1}{\ln\left(2 \frac{4(1+\sigma)}{\pi^2 \Gamma}\right)}. \quad (17)$$

The ASF of the Khokhlov solution [see Eq. (16)] is shown in Fig. 3 as a function of  $\sigma$  for three Gol'dberg numbers. Since the Khokhlov solution is only valid for  $3 < \sigma < \Gamma$ , the ASF values shown are truncated accordingly. For large  $\Gamma$  the waveform at  $\sigma = 3$  is approximately a sawtooth wave, which has an infinite ASF value. While the Khokhlov solution prediction is only valid up to  $\sigma = \Gamma$ , it is expected that the ASF would approach one as  $\sigma \rightarrow \infty$ , as thermoviscous absorption would lead to further unsteepening of the waveform.

### III. MEASUREMENT CONSIDERATIONS

The analytical expression for the ASF in the different regimes provide the first step in quantifying the relationship

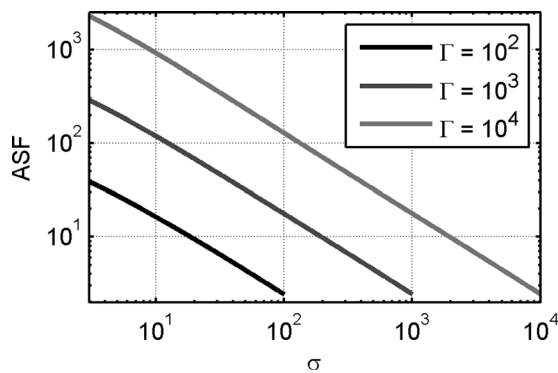


FIG. 3. Average steepening factor (ASF) of the Khokhlov solution as a function of  $\sigma$ , distance from the source over shock formation distance, for three values of Gol'dberg number.

between the ASF and nonlinearity in measured signals. The next step is to understand how the analytical expressions are affected by measurement considerations such as finite sampling rates and extraneous noise. Since real measurements are acquired at a finite rate, rapid pressure changes may not be adequately captured, and the resulting estimate of the ASF of a measured waveform may not adequately represent the true ASF. Another way the ASF of a measured waveform may be misrepresented is by the presence of noise not associated with the process of interest. For example, if one is measuring the noise radiating from a source in a windy environment, the wind noise would be considered measurement noise. This measurement noise can change the mean positive and negative slopes in a measured signal, and therefore significantly alter the estimated ASF.

The effects of finite sampling rates for initially sinusoidal signals propagating without linear losses and propagating with thermoviscous losses are first considered. Then, a simple numerical study of the effects of measurement noise on the estimate of the ASF of an initially sinusoidal signal is presented.

### A. Finite sampling rates

#### 1. Earnshaw solution

In order to calculate an ASF estimate of a waveform, we first find the regions of the waveform that are predicted to have positive time-derivatives and the regions that are predicted to have negative time-derivatives. The boundaries between the positive and negative slopes will have a slope estimate of zero. For a sine wave, the time at which this occurs,  $\tau_0$ , is found by solving

$$\begin{aligned} \frac{\Delta f}{\Delta \tau} &= \frac{f(\tau_0 + \Delta \tau) - f(\tau_0)}{\Delta \tau} \\ &= \frac{\sin(\omega(\tau_0 + \Delta \tau)) - \sin(\omega\tau_0)}{\Delta \tau} = 0, \end{aligned} \quad (18)$$

where  $\Delta \tau$  is time between measurements. We may solve Eq. (18) for  $\tau_0$  and obtain

$$\tau_0 = \frac{\pi}{\omega} \left( m + \frac{1}{2} - \frac{1}{f_r} \right), \quad (19)$$

where  $m = 0, \pm 1, \pm 2, \dots$ , and even values of  $m$  represent the transition from positive slope to negative slope estimates and odd values of  $m$  represent the transition from negative slope to positive slope estimates. The sample density,  $f_r$ , is the ratio of the sampling rate to the frequency of the initial sinusoid. When  $f_r$  is chosen to be an irrational number, over a long measurement time every possible discretely sampled slope will be represented. Therefore, due to the periodicity of the waveform, the irrational  $f_r$ , and the long measurement time, averaging the slopes between  $\tau = -\pi/2\omega - \pi/f_r\omega$  ( $\tau_0$  with  $m = -1$ ) and  $\tau = \pi/2\omega - \pi/f_r\omega$  ( $\tau_0$  with  $m = 0$ ) yields the average positive slope. Similarly, averaging the slopes between  $\tau = \pi/2\omega - \pi/f_r\omega$  ( $\tau_0$  with  $m = 0$ ) and  $\tau = 3\pi/2\omega - \pi/f_r\omega$  ( $\tau_0$  with  $m = 1$ ) will be the average negative slope that would be estimated with the same assumptions.

The method described for a sinusoidal wave may be extended to the case of an initially sinusoidal plane wave propagating according to the Earnshaw solution prior to shock formation. Since the nonlinear distortion of a waveform prior to shock formation depends only upon amplitude, the time delay between two points with the same amplitude will remain the same. This means the  $n$ th time at which the slope estimate will be zero,  $\tau_n$  will follow the distortion described by the Earnshaw solution, which is

$$\tau_n(\sigma) = \frac{\pi}{\omega} \left( n + \frac{1}{2} - \frac{1}{f_r} \right) - \frac{\sigma}{\omega} \cos\left(\frac{\pi}{f_r}\right) (-1)^n. \quad (20)$$

Assuming once again a long measurement time and an irrational  $f_r$ , we find the average positive slope estimate is

$$E \left[ \left( \frac{\Delta p}{\Delta \tau} \right)^+ \right] = \frac{1}{\tau_0 - \tau_{-1}} \int_{\tau_{-1}}^{\tau_0} \frac{\Delta p}{\Delta \tau} d\tau, \quad (21)$$

where  $\Delta p/\Delta \tau$  is the forward-difference estimate of the pressure derivative at a distance  $x$  from the source at the retarded time  $\tau$ . Similarly, the long-time average negative slope estimate is

$$E \left[ \left( \frac{\Delta p}{\Delta \tau} \right)^- \right] = \frac{1}{\tau_1 - \tau_0} \int_{\tau_0}^{\tau_1} \frac{\Delta p}{\Delta \tau} d\tau. \quad (22)$$

Since the integral of  $\Delta p/\Delta \tau$  over an entire period is zero, the integrals in Eq. (21) and (22) have the same magnitudes but opposite signs. Thus, the ASF estimate of the discretely sampled initially sinusoidal plane wave becomes

$$\text{ASF} = \frac{\pi + 2\sigma \cos(\pi/f_r)}{\pi - 2\sigma \cos(\pi/f_r)}, \quad 0 < \sigma < \frac{\pi}{2}. \quad (23)$$

The estimate of the ASF in Eq. (23) is plotted as a function of  $\sigma$  in Fig. 4(a) for several values of  $f_r$  (or sample-densities). For comparison, the exact ASF values from the Earnshaw solution assuming continuous sampling are also plotted. The relative errors between the continuously sampled ASF and the ASF estimates ( $1 - \text{ASF}_{f_r}/\text{ASF}_{\text{cont}}$ )

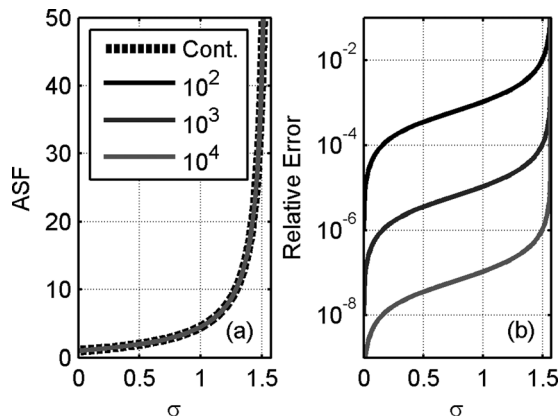


FIG. 4. (a) Average steepening factor (ASF) of an initial sinusoidal wave propagating according to the Earnshaw solution assuming continuous sampling for  $f_r = 10^2$ ,  $f_r = 10^3$ , and  $f_r = 10^4$ . (b) Error of the ASF estimate using discrete sampling relative to continuous sampling ( $1 - \text{ASF}_{f_r}/\text{ASF}_{\text{cont}}$ ).

are plotted in Fig. 4(b). The error plot shows that, at least in the pre-shock region, greater values of  $\sigma$  generate greater errors for a given sampling frequency. However, the errors are quite small. As seen by the darkest curve in Fig. 4(b), even  $f_r = 10^2$  only has about 10% error at the shock formation distance. If we assume that less than 1% error is sufficient precision, then it appears that  $f_r > 10^3$  is sufficient to estimate the ASF for initially sinusoidal plane waves propagating without linear losses prior to shock formation. Based on the trends of the ASF estimate errors, it seems likely that  $f_r > 10^4$  would be sufficient to estimate the ASF value for all  $\sigma$ . Another interesting feature of the plots of relative error in Fig. 4(b) is the regularity of the decay with respect to  $f_r$ . Assuming that  $f_r$  is large in Eq. (23) shows that the relative error decays as  $f_r^{-2}$ .

It is important to notice that close to  $\sigma = \pi/2$  the errors in Fig. 4 become very large. This dramatic loss of accuracy occurs as the total pressure rise time per period becomes small relative to sampling period. This undersampling of the pressure rise causes the estimate of the ASF to become significantly lower than the true value.

## 2. Khokhlov solution

Assuming the value of  $f_r$ , the sampling rate over the frequency of the initially sinusoidal plane wave, is irrational and the sample length is very long, the ASF of the discretely sampled Khokhlov solution can be found by evaluating Eq. (2) using Eqs. (21) and (22). The forward difference estimate of the slope of the discretely sampled Khokhlov solution at  $-\pi < \tau < \pi$ , which is needed to solve the integrals in Eqs. (21) and (22), is

$$\frac{\Delta p}{\Delta \tau} = \frac{p_0 [-\omega \Delta \tau + \pi (\tanh(\delta \omega (\tau + \Delta \tau)) - \tanh(\delta \omega \tau))]}{\Delta \tau (1 + \sigma)}, \quad (24)$$

where

$$\delta = \frac{\pi \Gamma}{2(1 + \sigma)}. \quad (25)$$

The limits of integration may be found by setting Eq. (24) equal to zero and solving for  $\tau$ . Calculating the maximum and minimum  $\tau$  values and noticing that the integrals in Eqs. (21) and (22) again have equal magnitude and opposite parity, and the duration of the negative slope in a period is  $2\pi/\omega$  minus the duration of the positive slope, so the ASF may be written

$$\text{ASF} = \frac{2\pi\delta}{\tanh^{-1}(\sqrt{B}/A)} - 1, \quad (26)$$

where

$$\begin{aligned} f_r &= \frac{2\pi}{\omega \Delta \tau}, \\ A &= f_r - \coth(2\pi\delta/f_r), \\ B &= 1 + f_r^2 - 2f_r \coth(2\pi\delta/f_r). \end{aligned} \quad (27)$$

The estimate of the ASF for the discretely sampled Khokhlov solution is plotted as a function of  $\sigma$  in Fig. 5(a) for several values of  $f_r$  (or sample-densities). For comparison, the exact ASF values assuming continuous sampling are also plotted. The relative errors between the continuously sampled ASF and the ASF estimates  $(1 - \text{ASF}_{f_r}/\text{ASF}_{\text{cont}})$  are plotted in Fig. 5(b). For the Gol'dberg number used for Fig. 5 ( $\Gamma = 1000$ ), using  $f_r = 10^4$  guarantees the ASF estimate of the Khokhlov solution will have less than 1% error for the entirety of the valid propagation range. The relative error using  $f_r = 10^3$  does not fall below 1% until about  $\sigma = 14$ , and the relative error using  $f_r = 10^2$  does not fall below 1% until about  $\sigma = 196$ . As the old-age regime begins at  $x = l_x$ , which for  $\Gamma = 1000$  is  $\sigma = \Gamma = 1000$ ,  $f_r = 10^2$ ,  $10^3$ , and  $10^4$  yield decent estimates of the ASF (estimates with relative errors less than 1%) well before this, where shocks are likely to be significant. As with the relative error of the initially sinusoidal plane wave propagating without linear losses, the relative error of the initially sinusoidal plane wave described by the Khokhlov solution also appears to fall off regularly with increasing values of  $f_r$ . Assuming  $f_r$  and  $\Gamma$  are large, the relative error of the ASF of the Khokhlov solution also decays as  $f_r^{-2}$ .

## B. Measurement noise

Often a measured waveform contains evidence of energy unassociated with the signal of interest or other features due to the measurement process; this will be referred to as measurement noise. It is desirable to know how measurement noise affects the estimation of the ASF of a measured waveform. The problem of finding the ASF of a signal containing measurement noise depends upon the amplitude, frequency content, and the statistics of the measurement noise. In this section we provide general insights into how the ASF depends on the amplitude and frequency of the measurement noise.

Consider the simple case of a “noisy” measurement of an initially sinusoidal wave propagating as a plane wave without losses. For the sake of simplicity, we assume the measurement noise is also sinusoidal but does not

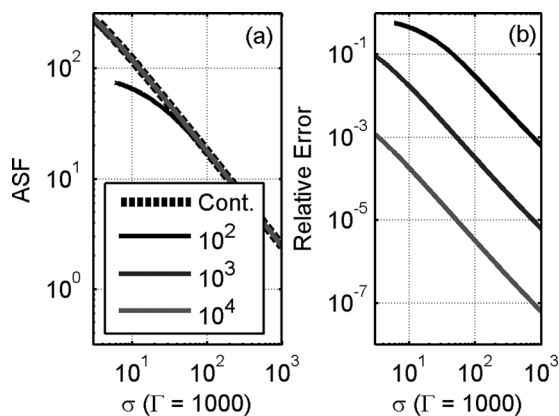


FIG. 5. (a) Average steepening factor (ASF) of the Khokhlov solution with a Gol'dberg number of 1000 assuming continuous sampling and assuming  $f_r = 10^2$ ,  $10^3$ , and  $10^4$ . (b) Error of the ASF estimate using discrete sampling relative to continuous sampling  $(1 - \text{ASF}_{f_r}/\text{ASF}_{\text{cont}})$ .

necessarily have the same frequency and is uncorrelated with the propagating signal. This situation could correspond to a propagating signal of interest being modified by an undesirable, strongly frequency dependent scattering process. The ASF of this noisy signal may be estimated numerically for several relative measurement noise frequencies and amplitudes. These estimated ASF values are plotted in Fig. 6 as a function of the ratio of the measurement noise frequency to the fundamental signal frequency for several signal-to-noise ratios (SNRs), at  $\sigma = 0.75$  and at  $\sigma = 0.95$ . For both propagation distances, the estimated ASF approaches the pure signal value as the SNR becomes large and as the frequency ratio becomes small.

The results shown in Fig. 6 may be qualitatively described by considering limiting cases. Measurement noise with very small relative frequencies may be considered a hydrostatic pressure change relative to the signal. Since the ASF is only a ratio of the slopes, the gradual change in overall pressure is insignificant relative to the signal, and so the noiseless ASF is approached. On the other extreme, as the measurement noise frequency becomes much greater than the fundamental frequency of the signal, the oscillation of the measurement noise dominates and the ASF estimate approaches 1. It is interesting to note that, for a given SNR, the relative frequency at which the ASF with measurement noise deviates from the pure signal case is the same for different values of  $\sigma$ . Additional comparisons at a variety of propagation distances (not shown) show that this critical relative frequency is a function solely of the SNR.

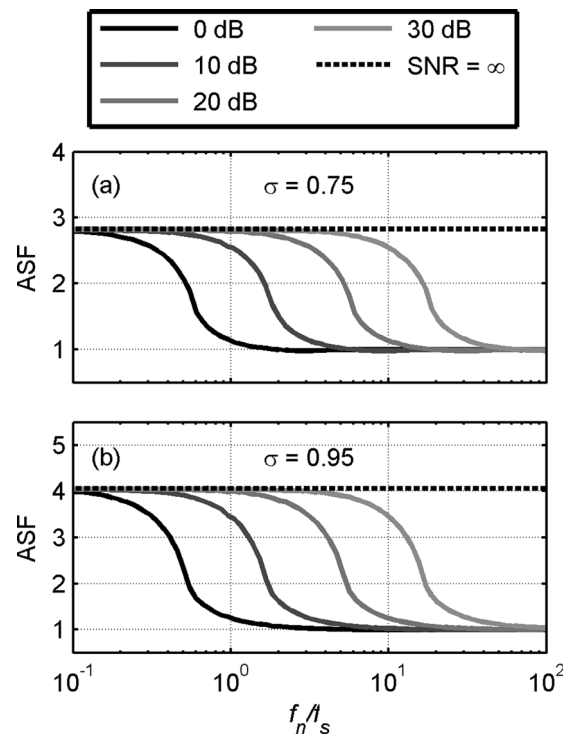


FIG. 6. Average steepening factor (ASF) of an initially sinusoidal plane wave propagating without losses to (a)  $\sigma = 0.75$  and (b)  $\sigma = 0.95$  (where  $\sigma$  is the distance over the shock formation distance) as a function of the frequency of the added measurement noise ( $f_n$ ) over the fundamental frequency of the signal ( $f_s$ ) for several signal to noise ratios (SNRs).

#### IV. APPLICATIONS

While the analytical expressions of the ASF derived in Secs. II and III are important benchmark cases, they are somewhat limited in scope. For example, the evolution of the ASF of an initially sinusoidal signal propagating with thermoviscous losses from the source to  $\sigma = 3$  and the ASF of initially Gaussian noise are not described. To gain insight into how the ASF evolves for more general waveforms and systems, we turn to numerical and experimental techniques. The following discussion covers a few examples and focuses on comparing these more realistic cases with the analytical ones and hence, better understanding of the behavior of the ASF.

##### A. Numerical simulations

This section first compares the ASF of initially sinusoidal waveforms with different amplitudes propagated numerically<sup>37</sup> with only thermoviscous absorption, with the analytical predictions from Secs. II and III to provide a benchmark for more complex cases. Then, the ASF of an initially sinusoidal waveform propagated with thermoviscous absorption is compared with the ASF of the same waveform propagated in a cylindrical duct environment. Finally, the ASF of an initially sinusoidal signal and the ASF of an initially Gaussian, broadband signal, both propagated with only thermoviscous absorption, will be compared.

The parameters for the numerical simulations are chosen to represent realistic conditions. All of the initial waveforms had a characteristic frequency of 1500 Hz and used a sampling rate of 204.8 kHz, therefore giving a value of  $f_r = 136.5$ . Each waveform used  $2^{18}$  samples, corresponding to 1.28 s of data. The broadband signal was generated by taking spectrally white Gaussian noise and applying a fourth-order Butterworth bandpass filter from 700 to 2300 Hz, with the arithmetic mean being 1500 Hz. The absorption coefficient used to simulate propagation in a cylindrical duct was derived using a cross-sectional radius of 2.54 cm (1.0 in) at a temperature of 293.15 K, an ambient pressure of 0.85 atm, and 20% relative humidity.<sup>38</sup> These conditions were chosen to be similar to the conditions of the experimental setup discussed below. The real part of the absorption coefficient in the duct at 1500 Hz was chosen to be the 1500 Hz absorption coefficient for the thermoviscous propagation cases. This ensures the characteristic absorption will be the same for all scenarios. A numerical, generalized, Burgers-type propagation scheme<sup>37</sup> was used to predict the nonlinear waveform evolution for one-dimensional propagation with either thermoviscous absorption or in a cylindrical duct environment. The ASF of a given waveform was estimated by using a forward difference numerical differentiation, calculating the mean of the positive and negative derivative values, and then taking the ratio of the average positive and negative slopes.

The numerically predicted evolution of the ASF of initially sinusoidal plane waves with Gol'dberg numbers  $\Gamma = 2$  and 20, propagating with thermoviscous absorption is shown in Fig. 7 along with the predicted ASF values from the Earnshaw (lossless) and Khokhlov ( $\Gamma = 20$ ) solutions. The variation in the Gol'dberg number comes from the initial

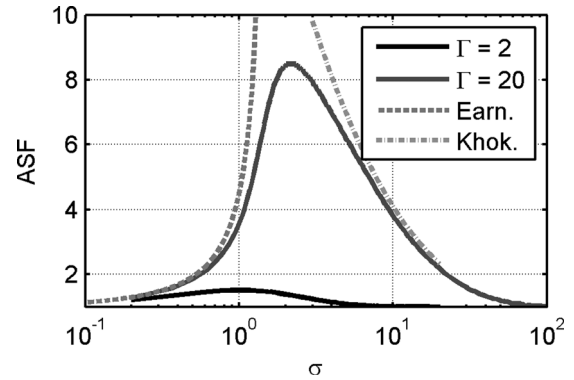


FIG. 7. Average steepening factor (ASF) of initially sinusoidal plane waves with  $\Gamma = 2$  or 20, numerically propagated with thermoviscous absorption as a function of distance over shock formation distance  $\sigma$ . The analytical ASF for the Earnshaw (Earn.) solution and for the Khokhlov (Khok.) solution with  $\Gamma = 20$  are shown for reference.

waveforms having differing amplitudes. In both cases, the ASF approaches that found for the Earnshaw solution for small  $\sigma$ . As the distance from the source increases, the numerically predicted ASFs depart from the Earnshaw solution due to the presence of absorption. The ASF of the  $\Gamma = 2$  wave departs from the lossless case more rapidly than the  $\Gamma = 20$  wave because absorption is more dominant for smaller Gol'dberg numbers. Since the Khokhlov solution is only valid for  $3 < \sigma < \Gamma$  with very large  $\Gamma$ , it is not valid for any part of the  $\Gamma = 2$  waveform, and it is not expected that the  $\Gamma = 20$  waveform would have the same ASF as the Khokhlov solution. This is demonstrated in Fig. 7. The greatest difference between the ASF of the  $\Gamma = 20$  waveform and the Khokhlov solution occurs at  $\sigma = 3$ . From the plots in Fig. 7 and other comparisons, the largest ASF values for initially sinusoidal signals with large Gol'dberg numbers propagating with thermoviscous absorption occurs between  $\sigma = \pi/2$  and  $\sigma = 3$ . For smaller Gol'dberg numbers, the maximum ASF value likely occurs closer to the source than this range suggests.

The ASF for the  $\Gamma = 20$  waveform shown in Fig. 7 is also shown in Fig. 8 along with the ASF for an initially

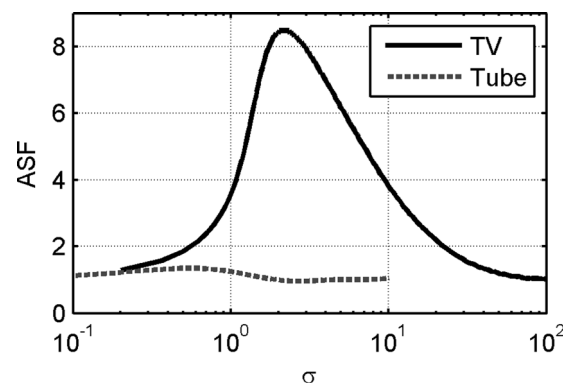


FIG. 8. Average steepening factor (ASF) of an initially sinusoidal plane wave numerically propagated with thermoviscous (TV) or tube-like (Tube) absorption as a function of distance over shock formation distance  $\sigma$ . The thermoviscous case has a Gol'dberg number of  $\Gamma = 20$ , while the tube-like absorption has a Gol'dberg number of  $\Gamma = 0.49$ , due to the increased absorption.

sinusoidal waveform propagating in a plane-wave tube environment. The waveform propagating in the tube was chosen to have the same amplitude as the  $\Gamma = 20$  waveform. Since the absorption associated with boundary layer losses is much higher at the fundamental frequency, the Gol'dberg number associated with the waveform propagating with tube-like absorption is only  $\Gamma = 0.49$ . The greater importance of absorption is apparent in Fig. 8 in that the greatest value of the ASF for the waveform propagating with tube-like absorption is 1.3, which is reached at  $\sigma = 0.6$ . Interestingly, in the tube-like absorption case the ASF actually drops below 1 for a little distance after the peak is reached. This may be due to the strong dispersion associated with boundary layer losses.<sup>39,40</sup>

We now consider the case of an initially broadband Gaussian noise propagating with thermoviscous losses. Before proceeding with the calculation of ASF, special care must be taken to define what  $\sigma$  means with respect to noise. The dimensionless distance  $\sigma$  for initially sinusoidal plane waves is the distance from the source over the lossless shock formation distance. Since the lossless shock formation distance is very case-sensitive for noise signals (it is actually infinitesimally small for Gaussian white noise, given the fact that the probability of increasingly steep slopes is never identically zero), we use a characteristic shock formation distance based off of the nonlinear distortion length defined by Gurbatov and Rudenko,<sup>41</sup>

$$\bar{x}_N = \frac{\rho_0 c_0^3}{\beta \omega_0 (\sqrt{2} p_{\text{rms}})}, \quad (28)$$

where  $\omega_0$  is the characteristic frequency and  $p_{\text{rms}}$  is the root-mean-square pressure. This deviates from the definition of Gurbatov and Rudenko by a factor of  $\sqrt{2}$ , so that as the bandwidth of the noise goes to zero  $\bar{x}_N \rightarrow \bar{x}$ . Thus, it is reasonable to have  $\sigma$  refer to  $x/\bar{x}_N$  for initially random signals. Furthermore, the Gol'dberg for random signals will be defined in this paper as  $\Gamma = (\alpha \bar{x}_N)^{-1}$ .

The ASF of an initially sinusoidal signal and the ASF of an initially broadband, Gaussian noise signal, both with  $\Gamma = 20$  and propagated using thermoviscous absorption, are shown in Fig. 9. It is clear that the random signal does not

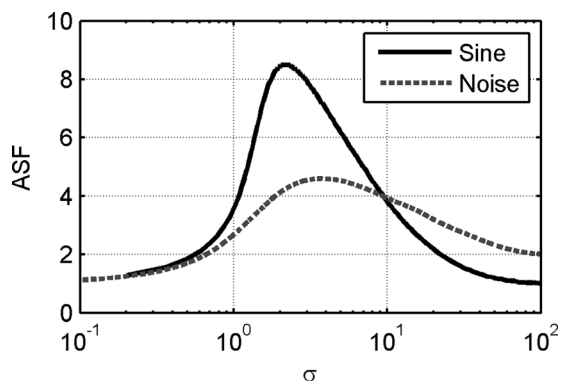


FIG. 9. Average steepening factor (ASF) of an initially sinusoidal signal and the ASF of an initially Gaussian broadband noise numerically propagated with thermoviscous absorption as a function of  $\sigma$ .

have ASF values as high as the initially sinusoidal signal and that the peak ASF values come farther from the source for noise than for initially sinusoidal signals (assuming the present definition of  $\bar{x}_N$ ). On the other hand, it seems that for large propagation distances, the ASF values for the noise signal do not decay as quickly as for the sinusoidal case. This suggests that, despite the presence of a small number of very large peaks in the noise waveform, which will quickly evolve into shocks, the ASF is dominated by the much larger number of lower amplitude peaks, which steepen more slowly. Therefore, the ASF may be more accurately described as a measure of the average steepness of a waveform.

## B. Plane-wave tube experiment

A plane-wave tube was used to experimentally verify some of the numerical results above. The tube was constructed of several 3.05 m long (10 ft), 2.54 cm (1 in) radius PVC pipes connected end to end with PVC couplers. The tube was driven at one end by a single BMS 4590 coaxial compression driver and was terminated anechoically with approximately a meter long piece of fiber-glass insulation at the other end. Small holes for microphones were drilled in the tube 0.4, 2.6, 5.6, 8.6, and 11.7 m from the driver. The microphones were 3.18 mm (1/8 in) 40DD G.R.A.S. pressure microphones, and they were mounted without grid caps in the tube such that the diaphragms were flush with the inner wall of the tube.

Portions of the waveforms measured for an initially sinusoidal 1500 Hz signal are shown in Fig. 10, with the corresponding harmonics shown in Fig. 11. The amplitude of the waveform measured 0.4 m from the driver is 547 Pa, which corresponds to a lossless shock formation distance of 6.6 m and a Gol'dberg number of about 3.3. This means the

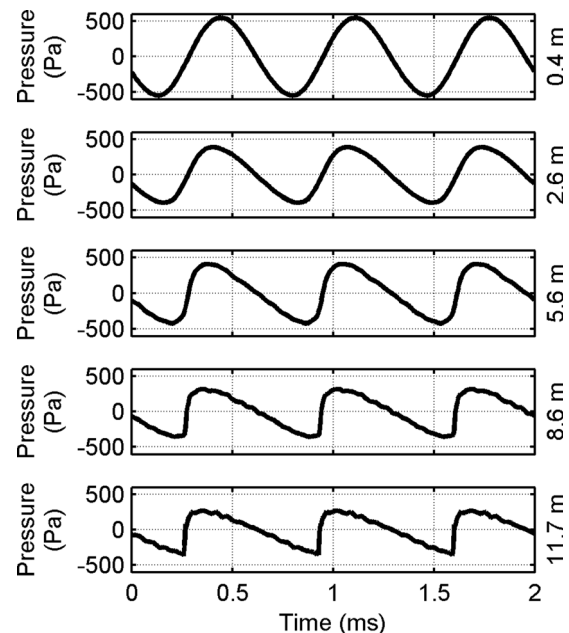


FIG. 10. Portions of initially sinusoidal plane waves measured in a plane-wave tube at five measurement locations, 0.4, 2.6, 5.6, 8.6, and 11.7 m from the source.

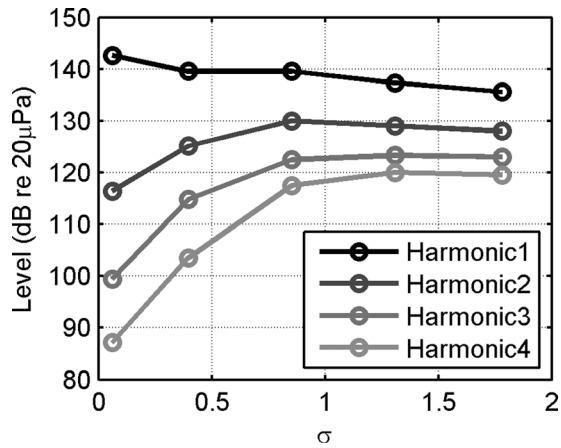


FIG. 11. The first four harmonics of the waveforms shown in Fig. 10 as a function of  $\sigma$ , distance from source over shock formation distance.

last microphone is located at  $\sigma = 1.78$ . As is expected for a plane wave with such amplitudes, the waveform demonstrates significant steepening at each measurement location, which is evidenced by the increase of harmonic energy with distance close to the source. The effects of the plane-wave tube absorption and dispersion are plainly evident in the rounding of the shocks in the waveforms from the farther microphones.<sup>39,40</sup> It is also important to notice that there appears to be some high-frequency measurement noise ( $\sim 12$  kHz), i.e., ringing, in the waveforms measured at 8.6 and 11.7 m from the source. This ringing does not appear in a numerical prediction of the 11.7 m waveform based on the waveform measured 0.4 m from the source, shown in Fig. 12. This noise may be due to high-frequency scattering at the imperfect junctions between the pipe segments.

The ASF of each measured waveform shown in Fig. 10 is plotted in Fig. 13. For comparison, the waveform measured 0.4 m from the source was numerically propagated from the source to  $\sigma = 2$ , and the ASF of the predicted waveform was calculated. The input waveform was first up-sampled by interpolation to 8 times the original sampling rate to minimize errors in the numerical prediction of the ASF associated with insufficient sampling rates. The numerically predicted ASF evolution, shown in Fig. 13, matches the ASF values of the measured waveforms quite well for

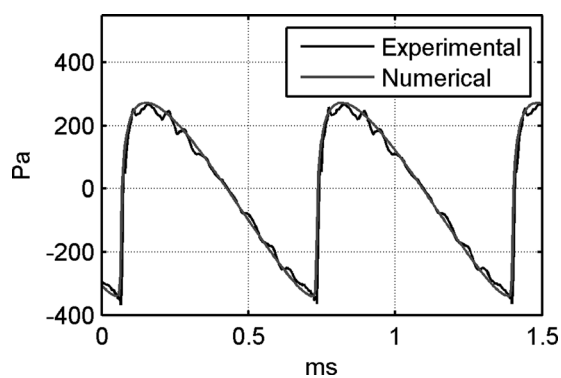


FIG. 12. A portion of the waveform measured in a plane-wave tube 11.7 m from the source with a portion of a waveform numerically propagated the same distance.

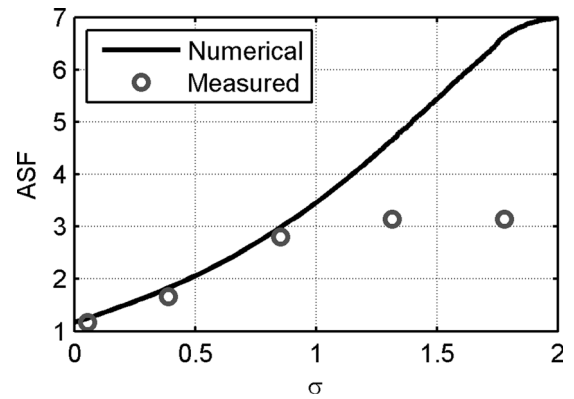


FIG. 13. Average steepening factor (ASF) of an initially sinusoidal signal measured at five normalized locations in a plane wave tube and the ASF predicted by numerically propagating the measured source signal as a function of normalized location. At the source, the waveform has a Gol'dberg number of approximately  $\Gamma = 3.3$ .

the first three locations. However, the ASF values of the waveforms measured at 8.6 and 11.7 m from the source are significantly lower than the numerical predictions. In fact, the 8.6 and 11.7 m ASF values are very similar to the 5.6 m ASF value, which is somewhat surprising, given that the 8.6 and 11.7 m waveforms appear significantly steeper than the 5.6 m waveform. A likely reason for the discrepancy between the prediction and experiment is the increased prevalence of small-amplitude, high-frequency ringing in the measured waveforms as shocks form. The small, positive slopes of the ringing serve to reduce and eventually limit the ASF value in this case. This example helps illustrate the impact of measurement noise (in this case, high-frequency ringing).

Gaussian-distributed, broadband (700–2300 Hz) noise signals were also propagated in the plane-wave tube experiment. The ASFs of noise signals measured in the plane wave tube along with the ASFs of the waveforms predicted by numerically propagating the waveform measured at the first location to the subsequent measurement locations are shown as a function of  $\sigma$  in Fig. 14. Two experiments are shown:

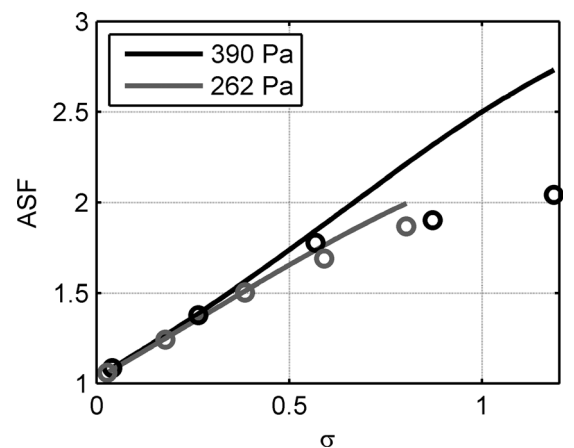


FIG. 14. Average steepening factor (ASF) of initially Gaussian noise measured at five normalized locations in a plane wave tube and the ASF predicted by numerically propagating the measured source signal as a function of normalized location. Two initial conditions are presented:  $\Gamma = 3.2$  (360 Pa) and  $\Gamma = 2.2$  (262 Pa) at the first measurement location, 0.4 m from the source.

one where the root-mean-square amplitude measured 0.4 m from the driver is about 360 Pa ( $\Gamma = 3.2$ ), and one where the root-mean-square amplitude at the same location is about 262 Pa ( $\Gamma = 2.2$ ). Similar to the numerical experiments above, the ASF grows more slowly for noise signals ( $\Gamma = 3.2$  case in Fig. 14) than for initially sinusoidal signals (Fig. 13). The ASF values of the measured noise diverge from the numerical prediction for the last two measurement locations, as was the case with the initially sinusoidal signal, but the difference between the prediction and measurement for noise is significantly lower than for the sinusoidal case. While there is still the ringing in the noise waveforms (not shown), the broader spectrum and lower ASF values in general may be contributing to the less severe discrepancy.

## V. CONCLUSIONS

This paper has introduced the average steepening factor (ASF) as a metric describing the average distortion that a propagating wave undergoes due to nonlinearity. The ASF, which is the inverse of the wave steepening factor defined by Gallagher,<sup>29</sup> has been shown to be a measure of the average effect of nonlinearity on the propagation of initially sinusoidal plane waves and initially broadband Gaussian noise. Analytical expressions of the ASF for the Earnshaw and Khokhlov solutions of the generalized Burgers equation, provide benchmarks that have been used to guide the interpretation of the values of the ASF obtained in numerical and experimental cases. It was shown that reductions in finite sampling rate do not significantly impact the estimation of ASF as long as the ratio of the sampling frequency to the characteristic frequency is at least  $10^2$  for waveforms without near-discontinuities. However, the ASF appears to be quite sensitive to extraneous measurement noise. Comparisons of the evolution of the ASF between initially sinusoidal signals and broadband Gaussian noise signals were made both numerically and experimentally. In both cases, the ASF grows more slowly for the noise than the initially sinusoidal case. The analytical, numerical, and experimental calculations in this study have increased the understanding of the behavior of the ASF as a metric for quantifying the average steepness of a waveform.

## ACKNOWLEDGMENTS

The authors gratefully acknowledge Brent O. Reichman for helping analyze some of the measured data used in this paper. This work was funded in part by a grant from the Office of Naval Research.

- <sup>1</sup>C. L. Morfey and G. P. Howell, "Nonlinear propagation of aircraft noise in the atmosphere," *AIAA J.* **19**, 986–992 (1981).
- <sup>2</sup>K. L. Gee, T. B. Gabrielson, A. A. Atchley, and V. W. Sparrow, "Preliminary analysis of nonlinearity in military jet aircraft noise propagation," *AIAA J.* **43**, 1398–1401 (2005).
- <sup>3</sup>K. L. Gee, V. W. Sparrow, M. M. James, J. M. Downing, C. M. Hobbs, T. B. Gabrielson, and A. A. Atchley, "The role of nonlinear effects in the propagation of noise from high-power jet aircraft," *J. Acoust. Soc. Am.* **123**, 4082–4093 (2008).
- <sup>4</sup>K. L. Gee, A. A. Atchley, L. E. Falco, M. R. Shepherd, L. S. Ukeiley, B. J. Jansen, and J. M. Seiner, "Bicoherence analysis of model-scale jet noise," *J. Acoust. Soc. Am.* **128**, EL211–EL216 (2010).

- <sup>5</sup>D. F. Pernet and R. C. Payne, "Non-linear propagation of signals in air," *J. Sound Vib.* **17**, 383–396 (1971).
- <sup>6</sup>O. V. Rudenko, "Interactions of intense noise waves," *Sov. Phys. Usp.* **29**, 413–447 (1986).
- <sup>7</sup>L. E. Falco, K. L. Gee, A. A. Atchley, and V. W. Sparrow, "Investigation of a single-point nonlinearity indicator in one-dimensional propagation," in *Forum Acusticum* (2005).
- <sup>8</sup>L. E. Falco, A. A. Atchley, and K. L. Gee, "Investigation of a single-point nonlinearity indicator in the propagation of high-amplitude noise," *AIAA Paper No. 2006-2529* (2006).
- <sup>9</sup>K. L. Gee, A. A. Atchley, L. E. Falco, and M. R. Shepherd, "Nonlinearity analysis of model-scale jet noise," in *19th International Symposium on Nonlinear Acoustics*, Tokyo, Japan, 2012.
- <sup>10</sup>B. P. Petitjean, K. Viswanathan, and D. K. McLaughlin, "Acoustic pressure waveforms measured in high speed jet noise experiencing nonlinear propagation," *Int. J. Aeroacoust.* **5**, 193–215 (2006).
- <sup>11</sup>W. J. Baars and C. E. Tinney, "Shock structures in the acoustic field of a mach 3 jet with crackle," *J. Sound Vib.* **333**, 2539–2553 (2014).
- <sup>12</sup>S. A. McNerny and S. M. Ölçmen, "High-intensity rocket noise: Nonlinear propagation, atmospheric absorption, and characterization," *J. Acoust. Soc. Am.* **117**, 578–591 (2005).
- <sup>13</sup>D. E. Gagnon, "Bispectral analysis of nonlinear acoustic propagation," Master's thesis, The University of Texas at Austin (2011).
- <sup>14</sup>S. N. Gurbatov and A. I. Saichev, "Degeneracy of one-dimensional acoustic turbulence at large Reynolds numbers," *Sov. Phys. JETP* **53**, 347–354 (1981).
- <sup>15</sup>S. N. Gurbatov, A. I. Saichev, and I. G. Yakushkin, "Nonlinear waves and one-dimensional turbulence in nondispersive media," *Sov. Phys. Usp.* **26**, 857 (1983).
- <sup>16</sup>S. N. Gurbatov, A. N. Malakhov, and N. V. Pronchatov-Rubtsov, "Evolution of higher-order spectra of nonlinear random waves," *Radiophys. Quantum Electron.* **29**, 523–528 (1986).
- <sup>17</sup>O. Rudenko and A. Chirkin, "Statistics of discontinuous noise waves in nonlinear media," *Akad. Nauk SSSR Dokl.* **225**, 520–523 (1975).
- <sup>18</sup>D. W. Webster and D. T. Blackstock, "Amplitude density of a finite amplitude wave," *J. Acoust. Soc. Am.* **65**, 1053–1054 (1979).
- <sup>19</sup>M. R. Shepherd, K. L. Gee, and A. D. Hanford, "Evolution of statistical properties for a nonlinearly propagating sinusoid," *J. Acoust. Soc. Am.* **130**, EL8–EL13 (2011).
- <sup>20</sup>M. B. Muhlestein and K. L. Gee, "Experimental investigation of a characteristic shock formation distance in finite-amplitude noise propagation," *Proc. Mtg. Acoust.* **12**, 045002 (2014).
- <sup>21</sup>K. L. Gee, V. W. Sparrow, A. A. Atchley, and T. Gabrielson, "On the perception of crackle in high-amplitude jet noise," *AIAA J.* **45**, 593–598 (2007).
- <sup>22</sup>S. A. McNerny, K. L. Gee, M. Downing, and M. M. James, "Acoustical nonlinearities in aircraft flyover data," *AIAA Paper No. 2007-3654* (2007).
- <sup>23</sup>P. Mora, N. Heeb, J. Kastner, E. Gutmark, and K. Kailasanath, "Impact of heat on the pressure skewness and kurtosis in supersonic jets," *AIAA J.* **52**, 777–787 (2014).
- <sup>24</sup>K. L. Gee, T. B. Neilsen, J. M. Downing, M. M. James, and S. A. McNerny, "Characterizing nonlinearity in jet aircraft flyover data," *Proc. Mtg. Acoust.* **12**, 040008 (2013).
- <sup>25</sup>K. L. Gee, T. B. Neilsen, J. M. Downing, M. M. James, R. L. McKinley, R. C. McKinley, and A. T. Wall, "Near-field shock formation in noise propagation from a high-power jet aircraft," *J. Acoust. Soc. Am.* **133**, EL88–EL93 (2013).
- <sup>26</sup>K. L. Gee, T. B. Neilsen, and A. A. Atchley, "Skewness and shock formation in laboratory scale supersonic jet data," *J. Acoust. Soc. Am.* **133**, EL491–EL497 (2013).
- <sup>27</sup>S. A. McNerny, "Launch vehicle acoustics. Part 2: Statistics of the time domain data," *J. Aircraft* **33**, 518–523 (1996).
- <sup>28</sup>K. L. Gee, R. J. Kenny, T. B. Neilsen, T. W. Jerome, C. M. Hobbs, and M. M. James, "Spectral and statistical analysis of noise from reusable solid rocket motors," *Proc. Mtg. Acoust.* **12**, 040008 (2013).
- <sup>29</sup>J. Gallagher, "The effect of non-linear propagation in jet noise," *20th Aerospace Sciences Meeting and Exhibit*, *AIAA Paper No. 82-0416* (1982).
- <sup>30</sup>W. J. Baars, C. E. Tinney, and M. S. Wochner, "Nonlinear noise propagation from a fully expanded mach 3 jet," *AIAA Paper 2012-1177* (2012).
- <sup>31</sup>W. J. Baars, "Acoustics from high-speed jets with crackle," Ph.D. thesis, The University of Texas at Austin (2013).

- <sup>32</sup>M. B. Muhlestein, "Analyses of nonlinearity measures in high amplitude sound propagation," Master's thesis, Brigham Young University (2013).
- <sup>33</sup>D. T. Blackstock, M. F. Hamilton, and A. D. Pierce, "Progressive waves in lossless and lossy fluids," in *Nonlinear Acoustics* (Acoustical Society of America, Melville, NY, 2008), Chap. 4, pp. 65–150.
- <sup>34</sup>D. T. Blackstock, "Connection between the Fay and Fubini solutions for plane sound waves of finite amplitude," *J. Acoust. Soc. Am.* **39**, 1019–1026 (1966).
- <sup>35</sup>J. S. Mendousse, "Nonlinear dissipative distortion of progressive sound waves at moderate amplitudes," *J. Acoust. Soc. Am.* **25**, 51–54 (1953).
- <sup>36</sup>D. T. Blackstock, "Thermoviscous attenuation of plane, periodic, finite-amplitude sound waves," *J. Acoust. Soc. Am.* **36**, 534–542 (1964).
- <sup>37</sup>K. L. Gee, J. M. Downing, M. M. James, R. C. McKinley, R. L. McKinley, T. B. Neilsen, and A. T. Wall, "Nonlinear evolution of noise from a military jet aircraft during ground run-up," AIAA Paper No. 2012-2258 (2012).
- <sup>38</sup>D. T. Blackstock, *Fundamentals of Physical Acoustics* (Wiley, New York, 2000), p. 513.
- <sup>39</sup>D. Weston, "The theory of the propagation of plane sound waves in tubes," *Proc. Phys. Soc. B* **66**, 695–709 (1953).
- <sup>40</sup>M. F. Hamilton, Y. A. Il'inskii, and E. A. Zabolotskaya, "Dispersion," in *Nonlinear Acoustics* (Acoustical Society of America, Melville, NY, 1998), Chap. 5, pp. 151–176.
- <sup>41</sup>S. N. Gurbatov and O. V. Rudenko, "Statistical phenomena," in *Nonlinear Acoustics* (Acoustical Society, Melville, NY, 1998) Chap. 13, pp. 377–398.